TightCap: 3D Human Shape Capture with Clothing Tightness

Xin Chen, Anqi Pang, Wei Yang, Lan Xu, Jingyi Yu[†]

Abstract—In this paper, we present TightCap, a data-driven scheme to capture both the human shape and dressed garments accurately with only a single 3D human scan, which enables numerous applications such as virtual try-on, biometrics and body evaluation. To break the severe variations of the human poses and garments, we propose to model the clothing tightness – the displacements from the garments to the human shape implicitly in the global UV texturing domain. To this end, we utilize an enhanced statistical human template and an effective multi-stage alignment scheme to map the 3D scan into a hybrid 2D geometry image. Based on this 2D representation, we propose a novel framework to predicted clothing tightness via a novel tightness formulation, as well as an effective optimization scheme to further reconstruct multi-layer human shape and garments under various clothing categories and human postures. We further propose a new clothing tightness dataset (CTD) of human scans with a large variety of clothing styles, poses and corresponding ground-truth human shapes to stimulate further research. Extensive experiments demonstrate the effectiveness of our TightCap to achieve high-quality human shape and dressed garments reconstruction, as well as the further applications for clothing segmentation, retargeting and animation.

Index Terms—Human shape capture, garment reconstruction, parametric human model.

✦

1 INTRODUCTION

W ITH the popularity of commodity 3D scanners such as Microsoft Kinect or ASUS Xtions, it has become increasingly common to create 3D human models in place of traditional 3D images. How to further reconstruct the human shape as well as dressed garments for challenging human and clothing variations evolves as a cutting-edge yet bottleneck technique, which has recently attracted substantive attention of both the computer vision and computer graphics communities.

In this paper, we focus on capturing the accurate human shape and the corresponding garments with only a single 3D scan, which is essential for numerous applications such as virtual try-on, biometrics, and body evaluation for gymnastics and sports. In reality, the human and clothing geometry can exhibit significant variations: borrowing jargon from clothing manufactures, clothing can be loose – large clothing-body gaps to allow a full range motion, fitted – a slimmer, athletic cut eliminating the bulk of extra fabric, and compression – ultra-tight, second-skin fit. As illustrated in Fig. 2, such a variety of clothing categories and looseness makes it a very challenging problem to capture the accurate human shape, let alone the variety of human postures and the further garment reconstruction. Earlier approaches [57], [63] utilize statistical body
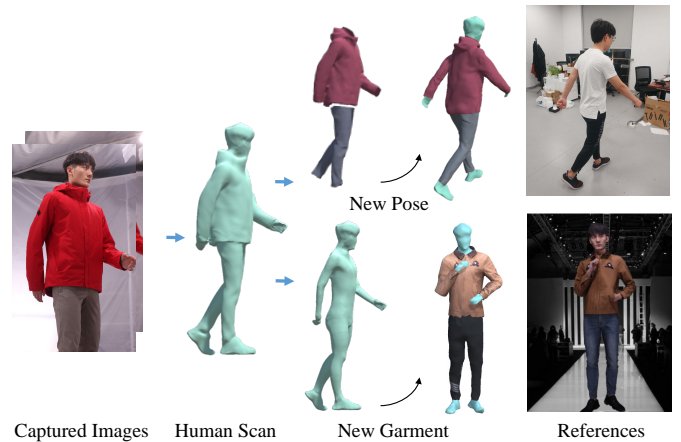

Fig. 1: Our method first reconstructs a clothed 3D scan from images, and predicts the underlying human body shape as well as segment the garments. This illustrates how we can support a range of applications related to multi-layer avatar generation with detected pose (Right top) and try-on with pre-segmented garment models (Right down).

- *Xin Chen, Anqi Pang are affiliated with the School of Information Science and Technology, ShanghaiTech University, Shanghai Institute of Microsystem and Information Technology, Chinese Academy of Science, as well as University of Chinese Academy of Sciences.*
  E-mail: {chenxin2, pangaq}@shanghaitech.edu.cn.
- *Lan Xu is with the Robotics Institute, Hong Kong University of Science and Technology, School of Information Science and Technology, ShanghaiTech University, as well as Dgene.*
  E-mail: lxuan@connect.ust.hk
- *Wei Yang is with University of Delaware, DGene and Google LLC.*
  E-mail: wyangcs@udel.edu.
- *Jingyi Yu is with the School of Information Science and Technology, ShanghaiTech University, Shanghai, China.*
  E-mail: yujingyi@shanghaitech.edu.cn.
- *[†] Corresponding author: Jingyi Yu.*

models, like SCPAE [4] and SMPL [30], to optimize the human shape parameters in the model space or the vertex displacements from the human template to the captured 3D scans. However, they are restricted by the generalization ability of the naked human template to handle various clothing geometry. On the other hand, the learning-based techniques [1], [7], [20], [23] have achieved significant progress recently to infer detailed geometry and body shape from images, but these image-based approaches suffer from scale ambiguity and inferior human shape accuracy.

In this paper, we propose TightCap, a data-driven approach to capture both human shape and dressed garments robustly

with only a single 3D scan, which outperforms existing state-of-the-art methods significantly. Our novel scheme introduces the clothing tightness which represents the displacements from various garments to the underlying human body model in a global UV texturing domain, so as to implicitly model the influence of various clothing categories, looseness, and human postures.

More specifically, to estimate the clothing tightness for various garment categories and human postures in a data-driven manner, we first map the captured human 3D scan into a global geometry image [17], called clothed-GI. To this end, we extend the statistical human model SMPL [30] by subdividing its geometry features around the garment boundary (e.g., neck, wrist, waist, ankle and so on) for the generalization to various clothing categories. Then, an effective multi-stage alignment scheme is adopted to warp the enhanced template to the captured scan, which jointly leverages the skeleton, silhouette, and geometry information in a coarse to fine manner to handle human pose and garment variations. Second, after alignment, we generate a hybrid feature embedding from the generated clothed-GI, including per-pixel texture, position, and normal. We further utilize a modified conditional generative adversarial network (GAN) to regress per-pixel clothing tightness in the UV texturing domain to handle human garment and posture variations, with the aid of a novel tightness formulation and a new 3D dataset that consists of a large variety of clothing including T and long shirt, short/long/down coat, hooded jacket, pants, skirt/dress, and the corresponding 3D human shapes. Finally, we propose an effective optimization scheme to reconstruct both the inner human shape and the multi-layer dressed garments accurately from the predicted tightness in the geometry image domain. Comprehensive experiments on both public and our captured datasets show that, compared with the state-of-the-art, with only a single captured 3D scan, our approach significantly improves the accuracy of human shape prediction, especially under various loose and fitted clothing. We further demonstrate how the recovered multi-layer human geometry can be applied to automatically segment clothing from the human body on 3D meshes as well as cloth retargeting and animation. To summarize, our main contributions include:

- A novel and superior human shape and garment capture scheme with a single captured 3D scan, which models clothing tightness to handle the garment and posture variations implicitly in the UV texturing domain.
- An effective multi-stage alignment approaches to enable clothed-GI generation from the captured scan with the aid of an enhanced statistical model.
- An novel tightness learning scheme based on a novel tightness formulation as well as an effective optimization scheme to recover both the human shape and garments.
- To stimulate further research, we make available our clothing tightness dataset (CTD) of totaling 880 human models with 228 different garments under various human postures as well as the ground truth human shapes.

2 RELATED WORK

Human and Garment Modeling. Most of the early works on human modeling can be categorized as multi-view stereo (MVS) vs. depth fusion based approaches. The former [13], [16], [36], [47] employs correspondence matching and triangulation . For example, Collet *et al*. [13] uses a dense set of RGB and IR video cameras, producing high quality 3D human results. The latter [8],
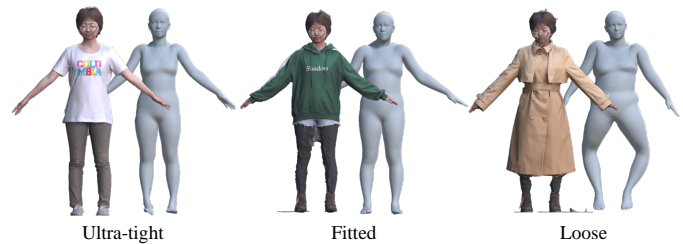

Fig. 2: The effectiveness of the parametric fitting model, such as SMPL [30], is weakened by clothes. From left to right, SMPL generates worse results (more unfit to underlying human body) for ultra-tight, fitted and loss clothes.

[15], [34], [59] uses active sensors such as structured light and Time-of-Flight (ToF) range scanning (e.g., Microsoft Kinect I and II, respectively) and are of a much lower cost. For example, Newcombe *et al*. [34] compensate for geometric changes due to motion captured from a single RGB-D sensor. DoubleFusion [60] presents a system to reconstruct cloth geometry and inner body shape based on the parametric body model. Their approach allows the subject to wear casual clothing and separately treat the inner body shape and outer clothing geometry. Recently, many works use learning based methods with statistical body models, like SMPL [30], to capture/reconstruct human with clothing [1], [7], [65] or recovery human body, like Pavlakos *et al*. [40] and HMR [23]. Also, there are some notable works [21], [22], [39], [54], from Carnegie Mellon University, capturing single or multiple 3D humans from 3D pose and body shape based on the panoptic studio or enhanced SMPL, especially SMPLX [39].

Garment modeling could be included in general human modeling, as we mentioned, but it always assumes the clothes and body skin as the same surface, like [1], [2]. They reconstruct clothed human from a single image or videos. Different from these methods, recent works [33], [42], [62] also propose the idea of the multi-layer human model for garment modeling. ClothCap [42] and SimulCap [62] both use SMPL as template model to help modeling garment from reconstructed human. For learning-based methods, DeepWrinkles [24] propose a data-driven framework to estimate garment wrinkles from body motion. Moreover, CAPE [31] and TailorNet [38] use learning based methods to generate a 3D mesh model of clothed people or directly proposes a neural garment model with pose, shape, and style.

Shape Under Clothing. Estimating body shape under clothing is more challenging. Existing methods employ a statistical or parametric 3D body model, like SCAPE [4] and SMPL [30], and require the subject wearing minimal or fitted clothing. The earlier work [6] builds on the concept of the visual hull under the assumption that the clothing becomes looser or tighter on different body parts as a person moves. They estimate a maximal silhouette-consistent parametric shape (MSCPS) from several images of a person with both minimal and normal clothing. Wuhrer *et al*. [53], estimate body shape from static scans or motion sequences by modeling body shape variation with a skeleton-based deformation. Their method requires fitted clothing. In general, human body shape estimation in wide and puffy clothing is significantly more difficult than in fitted clothing since even for humans. More recent approaches [18], [42], [63] attempt to align clothing on the human body model. Our approach also aims to align a parametric model, but we employ the geometry image analysis and exploit tightness
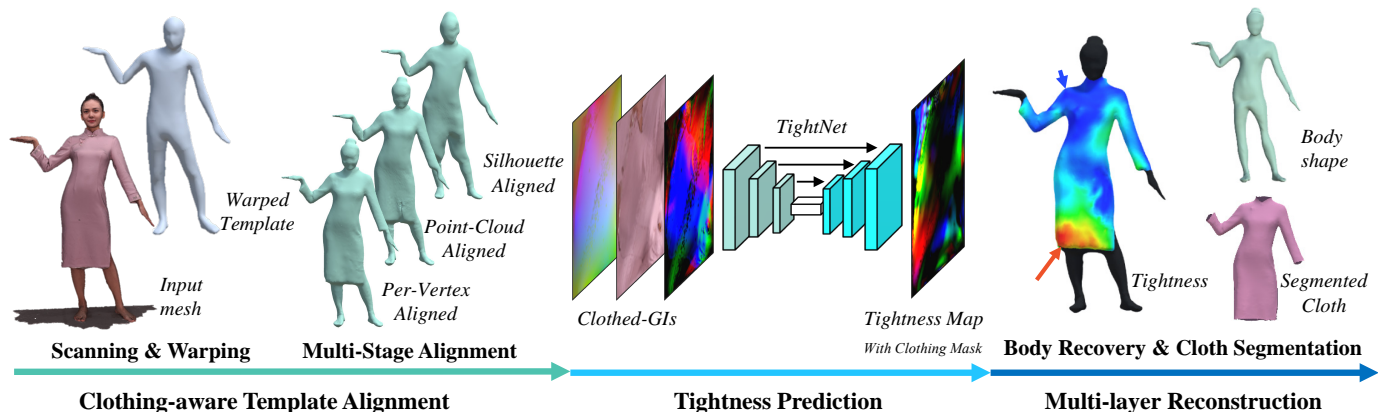
Fig. 3: The pipeline of TightCap. The first step is to warp our enhanced clothing-adapted SMPL with scanned mesh. Then, we deform warped mesh using *Multi-Stage Alignment*. After, we estimate the tightness map and clothing mask from mapped clothed-GI with *Tightness Prediction*. The final step, *Multi-layer Reconstruction* is to recover body shape from predicted tightness on the mesh, and segment cloth.

prediction for more reliable shape prediction.

For learning-based methods, [37], [41], [52] learn articulated body poses of humans from their occluded body parts via convolutional networks (ConvNets). [27] predicts body segments and landmarks from annotated human pose datasets, and conducts body pose estimation with clothing and 3D body fitting. Lassner *et al*. [26] present a generative model of the full body in clothing, but their work focuses more on appearance generation than body shape estimation. Especially, HMR [23] proposes an end-to-end ConvNet to recover the parameters of SMPL, for generating a 3D human body mesh from a single image. Pavlakos *et al*. [40] refine this similar generated body mesh by projecting it back to the 2D image for full-body pose and shape estimation. Their technique relies on parameter prediction from the body model and body pose accuracy. Most recently, Yang *et al*. [58] exploits the relation between clothing and the underlying body movement with data collected as the same actor in the same clothing, the same actor in different clothing, and different actors in the same type of clothing. ClothCap [42] estimates a minimally clothed shape and uses retargeting to map the body shape in different sizes and poses. DoubleFusion [60] use SMPL to estimate body shape as one layer of their double layer model.

Instead of modeling the variations of clothing and underlying body, such as Yang *et al*. [58] and Zhang *et al*. [63], our approach builds a GAN based technique to learn the tightness between the human body and the cloth layer. We also estimate both inner body shape and clothing segmentation from CTD dataset of different subjects in different clothing styles. There are also several works, such as Octopus [1] and Video Avatars [2], propose to use per-vertex displacements to compensate the gap between clothed and unclothed human model. However, their offsets/displacements do not consider the influence of various clothing types, and their main purpose is to reconstruct a clothed human with the template model, rather than to extract body shape. Instead, we take the tightness into consideration for both mesh alignment and shape recovery. Moreover, with the extract of the tightness, our approach can recover clothing and body shape from a single captured static mesh. Compared to mesh sequence based method, Zhang *et al*. [63], our approach using only a static mesh, which can leverage the commercial 3d sensors, such as Kinect and ToF cameras on mobile phones. Compared to single image based, like HMR [23]

and SMPL-X [39], our method has a more reliable and accurate body and clothing recovery.

3 OVERVIEW

Our goal in this paper is to reconstruct the human shape and corresponding garments accurately with a single captured 3D scan. To handle this challenging problem under the huge variations of clothing categories and human postures, we utilize the clothing tightness in a data-driven manner, which relies on a representative dataset with both clothed human scans and corresponding inner body shapes. Thus, we collect a new clothing tightness dataset (CTD) with dressed human meshes under various clothing and poses, which are reconstructed via a dome system equipped with 80 RGB cameras using the MVS approach [44] or a RGB-D sensor using DynamicFusion [34]. The corresponding ground truth naked human shapes are obtained via the same system and further manually re-posed and annotated by multiple professional artists. Fig. 3 illustrates the three high-level components of our algorithm pipeline, which achieves considerably more accurate body shape reconstruction results than the previous method.

Human Template Alignment. To model the garment and posture variations implicitly, a novel template alignment scheme is adopted to map the input 3D scan into the 2D clothed-GI. Our scheme relies on a garment-specific human template extended from the statistical model SMPL [30] (Sec.4.1), and a multi-stage alignment which jointly leverages the skeleton, silhouette and geometry information in a coarse to fine manner (see Sec.4.2).

Tightness Prediction. Based on the hybrid feature map from the above clothed-GI, we propose to predict the corresponding 2D clothing tightness map in a data-driven manner, which utilizes a novel tightness formulation (see Sec.5.1) and an effective learning framework based on conditional GAN, named TightNet (see Sec.5.2).

Multi-layer Reconstruction. Finally, we utilize the predicted tightness map to reconstruct the multi-layer human shape and dressed garments accurately via an optimization scheme based on Gaussian kernels (see Sec.5.3). Such multi-layer reconstruction results further enable various application such as immersive cloth retargeting and avatar animation.
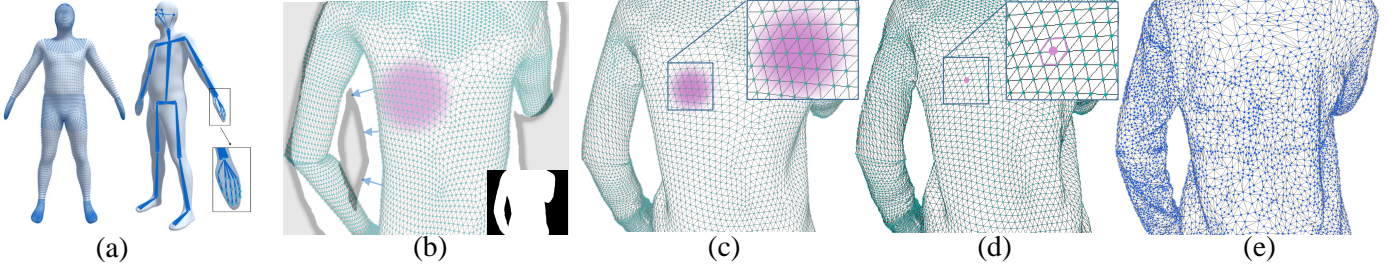
Fig. 4: Each stage of our alignment approach. (a) The template model for alignment. (b) The first stage, silhouette based deformation. (c) The second stage, point cloud based deformation. (d) The third stage, per-vertex deformation. (e) The referenced mesh (target mesh). The red regions indicate the different ranges of ED nodes.

4 HUMAN TEMPLATE ALIGNMENT

Under the canonical pose, the tightness between various clothing and body shapes share a similar distribution, e.g., the clothes tend to be loose around human oxter and crotch, and tight on shoulder and chest, which implies that the tightness of clothes with the underlying human body can be predicted in a data-driven manner. To this end, we transfer the input irregular 3D human scan into a global and regular 2D geometric image [17], called clothed-GI, to maintain the continuity of semantic human body distribution and implicitly model the variations of garments and human postures. To enhance the generalization to various clothing categories, a garment-specific statistical human model on top of SMPL [30] is adopted (Sec. 4.1) in our human alignment scheme. An effective multi-stage alignment is further adopted to warp the enhanced template to the captured scan, which jointly leverages the skeleton, silhouette, and geometry information in a coarse to fine manner to handle human pose and garment variations (Sec. 4.2). We also provide more implementation detail about how to generate the clothed-GI via UV mapping (Sec. 4.3) after the above multi-stage alignment for the clothing tightness training and prediction.

4.1 Clothing Adapted Human Template Model

The most successful parametric human models, i.e., the SMPL [30] and SMPL-X [39], focus on modeling the naked human body with various poses and shapes, which suffer from limited generation ability to handle clothing variations as demonstrated in Fig. 2. To this end, we extend the statistical human model SMPL [30] by subdividing its geometry features around the garment boundary (e.g., neck, wrist, waist, ankle and so on.) for the generalization to various clothing categories. We also simplify the template mesh around the ears, nose, and fingers for efficiency and rig the modified model with the skeleton defined by OpenPose [9], [45], i.e., 23 joints for the main body part and 21 joints for each hand, as shown in Fig.4 (a). The utilized clothing-adapted SMPL (CA-SMPL) model, denoted as $\mathcal{M}_T$, contains $N_\mathbf{M} = 14985$ vertices, $N_\mathbf{F} = 29966$ facets and $N_\mathbf{J} = 65$ joints, which is summarized as follows:

$$\mathcal{M}_\mathbf{T} = \left\{ \mathbf{M} \in \mathbb{R}^{N_\mathbf{M} \times 3}, \mathbf{F} \in \mathbb{R}^{N_\mathbf{F} \times 3}, \mathbf{J} \in \mathbb{R}^{N_\mathbf{J} \times 4+3} \right\}, \quad (1)$$

where $\mathbf{M}$, $\mathbf{F}$ and $\mathbf{J}$ denote the parameter sets of vertices, facets and joints, respectively. Here, the utilized skeleton parameters in the adopted human template are as follows:

$$\mathbf{J} = \left\{ \mathbf{\Theta} \in \mathbb{R}^{N_\mathbf{J} \times 3}, \mathbf{S} \in \mathbb{R}^{N_\mathbf{J}}, \mathbf{m} \in \mathbb{R}^3 \right\}, \quad (2)$$

including the joint angles $\mathbf{\Theta}$ with axis-angle representation, the scaling factors $\mathbf{S}$ of each joint along the bone direction, and the

global translation $\mathbf{m}$. Furthermore, let $M(\hat{\mathbf{J}})$ denote the skeletal motion of the human template after applied the joint parameters $\hat{\mathbf{J}}$, and $\hat{\mathbf{M}}$ represents the warped vertices of the template.

To enable robust alignment, we utilize the embedded deformation (ED) [48] by sampling the ED graph on the above enhanced human template, which is formulated as follows:

$$\mathcal{G} = \left\{ \mathbf{R} \in \mathbb{R}^{N_\mathbf{G} \times 3}, \mathbf{t} \in \mathbb{R}^{N_\mathbf{G} \times 3} \right\}, \quad (3)$$

where $N_\mathbf{G}$ is the number of nodes in ED graph. Then, the warping function G_k of the k-th node applied to a vertex $\mathbf{v}$ consists of the rotation $\mathbf{R}_k \in \mathbf{SO}(3)$ and the translate $\mathbf{t_k} \in \mathbb{R}^\mathbf{3}$, which is formulated as:

$$G_k(\mathbf{v}) = \mathbf{R}_k(\mathbf{v} - \hat{\mathbf{g}}_k) + \hat{\mathbf{g}}_k + \mathbf{t}_k, \quad (4)$$

where $\hat{\mathbf{g}}_k \in \mathbb{R}^3$ indicates the canonical position of the k-th node. Thus, the i-th vertex $\mathbf{v}_i, i \in [0, N_\mathbf{M})$ on the human template after applied the ED motion $\mathcal{G}$ is formulated as:

$$\mathbf{v}_i(\mathcal{G}) = G(\hat{\mathbf{v}}_i) = \sum_{k \in N_\mathbf{G}} \mathbf{w}_{i,k}^\mathbf{G} G_k(\hat{\mathbf{v}}_i). \quad (5)$$

Here $\hat{\mathbf{v}}_i$ is the canonical position of vertex i and $\mathbf{w}_{i,k}^\mathbf{G}$ is the skinning weight between the i-th vertex and the k-th ED node according to the Euclidean distance. Please kindly refer to [48] for more details about the setting of skinning weight.

4.2 Multi-Stage Alignment

To transfer the input irregular 3D human scan into the consistency human template, which shares the same topology for various garment categories and human postures, a novel multi-stage alignment scheme is adopted. Note that our scheme consists of the silhouette based, point cloud based and per-vertex deformation stages to optimize the non-rigid motions from the enhanced human template to the input 3D scan in a coarse to fine manner, as illustrated in Fig. 4.

Human Scan Reconstruction. Our raw 3D human scans can be captured using a multi-view dome system or a single-view depth sensor. For the former setting, we reconstruct using MVS approach [44] from multi-view human images captured by a dome system equipped with 80 cameras. We also estimate the 2D human joints for each image as in [9], [45] and obtain the 3D joints through triangulation as in [50] for initialization. The other setting is to reconstruct non-rigidly deforming human from commodity sensors, like ToF cameras on mobile phones and Kinect. We implement DynamicFusion [34] as our reconstruction method to acquire dynamic human scans. We also estimate the 2D human

joints for this single view and project it to depth map as our rough 3D joints. Our multi-stage deformation scheme can adapt to different application settings. More technical details for each stage are provided as follows.

Silhouette based deformation. We first align the enhanced template with the silhouette information from the captured scan using a coarse ED-graph to handle error prone places due to holes or noise on the raw human scan. To fetch the silhouette information, we utilize a virtual capture system with $N_\mathcal{C} = 30$ virtual cameras to view different areas of the captured 3D mesh. Note that for capturing the neck, ankles, and wrists, we set two virtual cameras orthogonal to each other. Besides, five cameras with different view angles are arranged to capture the upper and lower body torso, respectively. The resulting virtual camera setting is formulated as follows:

$$\mathcal{C} = \left\{ \left(\mathbf{c}_j \in \mathbb{R}^6, w_j^\mathcal{C} \in \mathbb{R}^1 \right) | j \in [0, N_\mathcal{C}) \right\}, \qquad (6)$$

where $\mathbf{c}_j$ denotes extrinsic parameters of a camera and $w_j^\mathcal{C} \in [0.5, 1]$ represents the weighting factor for two different camera positions (0.5 for the torso regions and 1 for capturing limbs). Such a semantic weighting strategy further improves the alignment results, especially for those boundary regions. We first warp the original human template model $\mathcal{M}_T$ with the rough 3D joints $\mathbf{J}_{mv}$ as our initial mesh for the following alignment. Inspiring by previous silhouette deformation method [55], we render the high resolution silhouette masks of the captured scan for all the virtual views and phrase the coarse-level alignment by solving the following non-linear least squares optimization problem:

$$E_\mathrm{S}(\mathcal{G}) = E_\mathrm{mv}^\mathrm{S}(\mathcal{G}) + \lambda_\mathrm{reg}^\mathrm{S} E_\mathrm{reg}^\mathrm{S}(\mathcal{G}). \qquad (7)$$

Similar to [55], our multi-view silhouette based data term E_mv^S measures the 2D point-to-plane misalignment:

$$E_\mathrm{mv}^\mathrm{S}(\mathcal{G}) = \sum_{j \in \mathcal{C}} \frac{w_j^\mathcal{C}}{|\mathbf{v}_j^\mathrm{S}|} \sum_{k \in \mathbf{v}_j^\mathrm{S}} \|\mathbf{n}_k^\mathrm{T} \cdot (P_j(\mathbf{v}_i(\mathcal{G})) - \mathbf{p}_k)\|_2^2, \qquad (8)$$

where $\mathbf{v}_j^\mathrm{S}$ is the vertex set of virtual silhouettes of the input scan and $P_j(\cdot)$ is the projection function of the j-th camera. For each silhouette point $\mathbf{p}_k \in \mathbb{R}^2$ with the 2D normal $\mathbf{n}_k \in \mathbb{R}^2$, we search its corresponding deformed vertex in the utilized human template, denoted as $\mathbf{v}_i$, found via a projective look-up method in an Iterative Closest Point (ICP) manner.

Similar to [46], the regularity term $E_\mathrm{reg}^\mathrm{S}$ produces locally as-rigid-as-possible (ARAP) motions to prevent over-fitting to the 3D scan input, which is formulated as:

$$E_\mathrm{reg}^\mathrm{S}(\mathcal{G}) = \sum_{k \in \mathcal{G}} \sum_{n \in \mathcal{N}_k} w_{k,n}^\mathcal{N} \|(\mathbf{g}_k - \mathbf{g}_n) - \mathbf{R}_k (\hat{\mathbf{g}}_k - \hat{\mathbf{g}}_n)\|_2^2, \qquad (9)$$

where $\mathcal{N}_k \in \mathcal{G}$ is the 1-ring neighbourhood of the k-th ED node and $w_{k,n}^\mathbf{N}$ denotes the KNN weight between the k-th and n-th nodes. For each ICP iteration, the resulting optimization problem in Eq.(7) is solved effectively using the Conjugate Gradient method. Let $\mathbf{M}_S$ denote the vertices of the deformed template after the silhouette-based optimization.

Point cloud based deformation. After the above silhouette based alignment, we re-sample a finer ED graph to model the fine-detailed geometry information in the input scan. For clarity and simplification, we reuse $\mathcal{G}$ to represent the ED motion from the previous results $\mathbf{M}_S$ to the input 3D mesh. Then, the full energy function for current fine-detailed alignment is formulated as:

$$E_\mathrm{D}(\mathcal{G}) = E_\mathrm{data}^\mathrm{D}(\mathcal{G}) + \lambda_\mathrm{reg}^D E_\mathrm{reg}^\mathrm{D}(\mathcal{G}). \qquad (10)$$

Here, the data term $E_\mathrm{data}^\mathrm{D}(\mathcal{G})$ measures the fitting from $\mathbf{M}_S$ to the input mesh, which is formulated as the sum of point-to-point and point-to-plane distances:

$$\begin{aligned} E_\mathrm{data}^\mathrm{D}(\mathcal{G}) =& \lambda_\mathrm{point}^\mathrm{D} \sum_{i \in \mathbf{M}} \|\mathbf{v}_i(\mathcal{G}) - \mathbf{v}_i^c\|^2 + \\ & \lambda_\mathrm{plane}^\mathrm{D} \sum_{i \in \mathbf{M}} (\mathbf{n}_i^\mathrm{T}(\mathcal{G}) \cdot (\mathbf{v}_i(\mathcal{G}) - \mathbf{v}_i^c)) \end{aligned} \qquad (11)$$

where $\lambda_\mathrm{point}^\mathrm{D}$ and $\lambda_\mathrm{plane}^\mathrm{D}$ are the weights to balance two kinds of distances; $\mathbf{n}_i(\mathcal{G})$ represents the normal of the deformed vertex $\mathbf{v}_i(\mathcal{G})$. Note that for each $\mathbf{v}_i(\mathcal{G})$, its corresponding point $\mathbf{v}_i^c$ in the scan is found via the same look-up method in an ICP manner.

The regularity term $E_\mathrm{reg}^\mathrm{D}(\mathcal{G})$ here shares the same formulated as the one in Eq.(9) and the full energy is solved using the same conjugate gradient solver. After this point cloud based alignment on a finer scale, the vertices of the deformed template are denoted as $\mathbf{M}_D$.

Per-vertex deformation. Finally, we refine the deformation from ED graph-based non-rigid result $\mathbf{M}_D$ to the input 3D mesh via per-vertex optimization, so as to improve the alignment accuracy especially for those local regions with fine details like clothing wrinkle and boundary, which is formulated as follows:

$$E_\mathrm{V}(\mathbf{M}) = E_\mathrm{data}^\mathrm{V}(\mathbf{M}) + \lambda_\mathrm{reg}^\mathrm{V} E_\mathrm{reg}^\mathrm{V}(\mathbf{M}). \qquad (12)$$

Here, similar to Eq.(11), the data term $E_\mathrm{data}^\mathrm{V}$ further measures the per-vertex fitting by minimizing the both the point-to-point and point-to-plane distances:

$$\begin{aligned} E_\mathrm{data}^\mathrm{V}(\mathbf{M}) =& \lambda_\mathrm{point}^\mathrm{V} \sum_{i \in \mathbf{M}} \|\mathbf{v}_i - \mathbf{v}_i^c\|^2 + \\ & \lambda_\mathrm{plane}^\mathrm{V} \sum_{i \in \mathbf{M}} (\mathbf{n}_i^\mathrm{T} \cdot (\mathbf{v}_i - \mathbf{v}_i^c)). \end{aligned} \qquad (13)$$

We utilize the same regularity term $E_\mathrm{reg}^\mathrm{V}$ from [55] to prevent over-fitting to the 3D input scan. let $\mathbf{M}_V$ denote the final optimized vertices of the human template. Fig. 4 shows the intermediate alignment results of all these stages, which demonstrates the effectiveness of our multi-stage alignment scheme. After the multi-stage alignment, we obtain a deformed human template that is not only fitted to the captured 3D human scan but also owns the global consistent topology.

4.3 Geometry Image Representation

Though it's possible to predict the tightness directly on the 3D mesh using techniques like GCN [29], it consumes much more computational resources and is generally harder to train. Instead, we map the clothed 3D body mesh with the consistent topology into a regular 2D UV image, which has been proved to be effective in previous works [3], [25], [56].

There are many methods to generate a 2D mapping from 3D mesh ways. We choose two representative methods for comparison. One is the mapping approach of the geometry image [17] with gapless filling but relative large distortions denoted as $M_{GI}(\cdot)$. The other method is OptCuts [28], denoted as $M_{Opt}(\cdot)$, which automatically seeks the best seam for cutting and generate an image with lower distortion but contains gap area. Fig. 5 illustrates
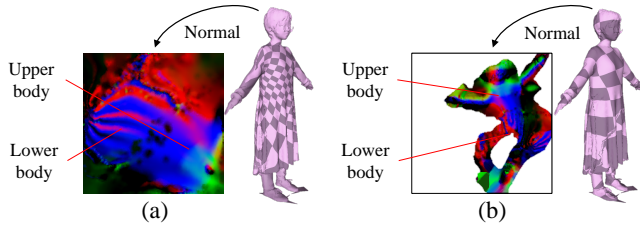
Fig. 5: The comparison of two feature map with different mapping methods. (a) The normal map using geometry image [17]. (b) The normal map using OptCuts algorithm [28].

the mapping results for both methods, and we utilize the geometry image [17] to achieve a more smooth feature representation. A quantitative comparison of these two methods for our full pipeline is provided in Sec. 6.2. To generate consistent 2D feature embeddings, we map the positions, normals, and RGB colors of each vertex into its 2D map using the mapping approach [17]. Linear interpolation is further conducted to fill the hybrid 2D clothed geometry image, which is denoted as clothed-GI.

5 TIGHTNESS PREDICTION

Previous human reconstruction methods, including methods based on scanned depth map(s) [13], [15], [34], [35], and silhouette(s) [5], [10], [11], [14], [32], [55], represent the human body as a single layer. Recently, [33], [42], [61], [62], [63] proposed the idea of multi-layer body shape recovery. We extend this idea and define a novel clothing tightness formulation, which describes the relationship between the underlying human body shape and the various garment layers (Sec. 5.1). Subsequently, we propose a conditional GAN to predict the clothing tightness in a data-driven manner, based on the 2D hybrid clothed-GI input and our novel tightness formulation. (Sec.5.2) We also introduce an effective optimization scheme to reconstruct both the inner human shape and the multi-layer dressed garments accurately from the predicted tightness in the geometry image domain (Sec. 5.3).

5.1 Tightness measurement

Similar to previous human modeling methods [1], [2] which models the displacements from the body template SMPL to the outer garment surface, we introduce the clothing tightness to measure the displacements form various garments to the underlying human body model. Recall that our clothing tightness dataset (CTD) contains both the dressed human meshes under various clothing and poses with the ground-truth underlying body models. To model the tightness from clothing layer to the real body layer using our CTD dataset, a straight-forward formulation is to align our enhanced SMPL model in Sec.4.1 to both the dressed mesh and the corresponding inner body mesh simultaneously using our multi-stage alignment method in Sec.4.2. Then, the per-vertex tightness is formulated on top of these two non-rigid aligned human templates which share the same topology:

$$\mathbf{T}_i = \mathbf{v}_i - \mathbf{v}_i^c. \tag{14}$$

Here, $\mathbf{v}_i$ and $\mathbf{v}_i^c$ are the i-th vertex of the two templates aligned to the clothing layer and the body layer, respectively. Note that the direction of $\mathbf{T}_i$ indicates the corresponding pairs from clothing to the inner body shape, while its magnitude is the euclidean distance
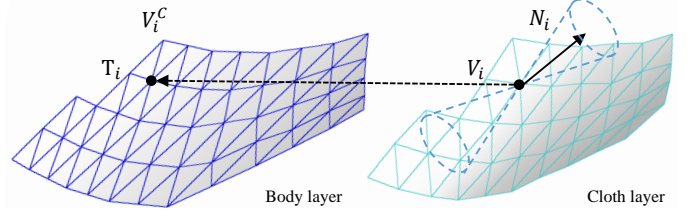

Fig. 6: Illustration of tightness $\mathbf{T}_i$ of vertex i on mesh.

between the two corresponding vertices. We can further define the tightness matrix, denoted as $\mathcal{T}$, on top of our enhanced SMPL model as follows:

$$\mathcal{T} = \left\{ \mathbf{T} \in \mathbb{R}^{N_\mathbf{M} \times 3} \right\}, \tag{15}$$

where $\mathbf{M}$ is the vertex matrix of the template with $N_\mathbf{M}$ vertices.

However, this straight-forward formulation above fails to model the exact correspondences between the clothing layer and the body layer, because the two non-rigid alignments from the template to the dressed mesh and the inner body model are performed totally independently, and the one-to-one correspondences are fragile to the alignment error. To this end, we formulate the tightness as the one-to-many correspondences between the human template aligned to the clothing layer and the ground-truth body model directly, jointly considering the direction and distance information of the clothing layer. For a vertex $\mathbf{v}_i$ on the aligned human template of the dressed mesh, we calculate its approximated tightness $\hat{\mathbf{T}}_i$ as follows:

$$\hat{\mathbf{T}}_\mathbf{i} = \frac{\sum_{\mathbf{v}_r^c \in \mathcal{N}_1^c} K_G(\mathbf{v}_i - \mathbf{v}_r^c) + \sum_{\mathbf{v}_d^c \in \mathcal{N}_2^c} K_G(\mathbf{v}_i - \mathbf{v}_s^c)}{||\mathcal{N}_1^c|| + ||\mathcal{N}_2^c||}. \tag{16}$$

Here, the one-to-many correspondence set $\mathcal{N}_1^c$ denotes the local vertices set of the ground-truth human body shape found via a ray-tracing operation along the normal direction of $\mathbf{v}_i$ within a double-cone with an aperture of 30 degrees, while $\mathcal{N}_2^c$ is the set of the 20 closest vertices of $\mathbf{v}_i$ in the ground-truth body mesh in terms of Euclidean distance, as shown in Fig.6. Note that $K_G(\cdot)$ is the Gaussian weighting function based on the angle between two vertex normals to enable smooth tightness estimation.

After the above tightness estimation from the dressed template to the ground-truth body model, we further apply the same strategy from the template aligned with the ground-truth body model to the raw dressed mesh and combine such bi-directional estimations to obtain the ground-truth 3D clothing tightness with the same topology of the enhanced SMPL template. Then, by using the same mapping operation in Sec.4.3, we generate the tightness map in the geometry image domain so as to enable end-to-end learning of the clothing tightness and implicitly to model the influence of various clothing categories, looseness, and human postures.

5.2 TightNet architecture

Based on the tightness map above and the hybrid 2D feature map from Sec. 4.3 in the global geometry image domain, we propose to train a Pixel2Pixel-style [19] convolutional neural network, denoted as TightNet, to infer the clothing tightness in an end-to-end manner. In the following, we provide more details about the input/output pair, the used network architectures, losses, and training schemes.

The input to our TightNet is the hybrid feature embedding in the clothed-GI from the raw 3D scan, including the vertex positions, normals, and RGB colors, while the output consists of the predicted tightness as well as the masks for both the upper and lower garments, so as to enable further multi-layer garment reconstruction. Note that for those clothing categories such as skirt and dress, the mask of the lower garment is set to be zero. Thanks to our unique 2D mapping scheme based on geometry image [17], both the input and output share the same semantic 2D structure, so as to implicitly handle the huge variations for clothing categories, garment looseness, and human postures.

The network in our TightNet is a conditional Generative Adversarial Network (Pixel2Pixel) [19], which learns a mapping from the input hybrid image and random noise vector. More specifically, the generator is U-Net [43] encoder-decoder structure with skip connections between convolution-ReLU-batch norm down- and up-sampling layers, which can share information between the input and output. In our discriminator, we utilized PatchGAN [19] discriminator and normal full image GAN discriminator. Since the high-frequency structure is not important in our task, we further normalize the full image GAN discriminator with a pyramid structure. We train the TightNet with the well-established L1-loss instead of L2-loss for fewer blurring artifacts. Benefiting from our tightness predictor, we can extract the hidden information between different clothing appearances and the tightness, while the input positions and normals also help our predictor to consider the effect of the current human pose.

5.3 Shape recovery under clothing

Based on the clothing tightness and mask prediction above, we propose an effective optimization scheme to reconstruct both the inner human shape and the multi-layer dressed garments accurately.

Shape recovery. Recall that our clothing tightness indicates the displacements from the garment layers to the inner human body layer. To cover the body shape from the tightness prediction, we first utilize the inverse function of the mapping $M_{GI}^{-1}(\cdot)$ in Sec.4.3 to generate the per-vertex tightness $\hat{\mathcal{T}}$ on the final aligned template mesh $\mathbf{M}_V$, where $\hat{\mathcal{T}} = \left\{ \hat{\mathbf{T}} \in \mathbb{R}^{N_\mathbf{M} \times 3} \right\}$. Then, a straight-forward solution to obtain the inner body shape $\mathbf{M}$ based on our tightness formulation is as follows:

$$\mathbf{M} = \mathbf{M}_V + \hat{\mathbf{T}}. \tag{17}$$

However, such solution above suffers from the tightness estimation error especially for those local regions around oxter and crotch under unusual human poses, leading to visually unpleasant body shape recovery. To this end, we propose a simple and effective optimization scheme to estimate a smoother body shape by solving the following least-squares energy function:

$$\begin{aligned} E_{\text{body}}(\mathbf{M}) =&\lambda_{fit}(\mathbf{M}_V + \mathbf{T} - \mathbf{M})+ \\ &\lambda_{smooth}(\mathbf{M} - K_G(\mathbf{M}))+ \\ &\lambda_{reg}(\mathbf{M} - \mathbf{M}_{warp}). \end{aligned} \tag{18}$$

Here the first data term utilizes our tightness formulation similar to Eq.(17), while the second term enables smooth body shape estimation via the same Gaussian kernel $K_G(\cdot)$ defined in Eq.(16). In the final regular term, the warped vertex matrix $\mathbf{M}_{warp}$ denotes the warped body template after the first ICP iteration of the first stage optimization in our multi-stage alignment in Sec. 4.2. Such

Fig. 7: Sample data from our dataset: three real human subjects with scanned body shape meshes, the segmented clothes, and one synthetic model (rightmost) for pre-training.

regular term forces the optimized body shape to be closed to the utilized human template to penalize unnatural body shape. All the parameters for these three terms are empirically set to be is 1, 0.1, and 0.05, respectively. Finally, by solving the least-squares problem in Eq.(18), we reconstruct an accurate and visually pleasant body shape of the input 3D human scan.

Clothing segmentation. Besides the body shape recovery above, we utilize the output multiple garment masks from our TightNet to automatically segment clothing from human body on 3D meshes so as to enable further cloth retargeting or animation applications. Since the output masks are not accurate enough to segment the clothing directly in the 3D space, we utilize the following integer linear optimization in [42] to solve the per-vertex clothing label $v_i \in \mathbf{v}$ for each vertex in our final aligned template mesh $\mathbf{M}_V$:

$$E_{\text{cloth}}(\mathbf{v}) = \sum_{i \in \mathcal{T}} \varphi_i(v_i) + \sum_{(i,j) \in \mathcal{T}} \psi_{ij}(v_i, v_j). \tag{19}$$

To enable fully automatic segmentation, we replace the manually defined garment prior of the original optimization in [42] with our predicted garment masks from TightNet. Please kindly refer to [42] for more details about how to solve the energy function above.

6 EXPERIMENTAL RESULTS

In this section, we evaluate our method on a variety of challenging scenarios. We first report the implementation of the details of our pipeline and utilized datasets, followed by the evaluation of our main technical contributions as well as the comparison with previous state-of-the-art methods, both qualitatively and quantitatively. The applications and limitations regarding our approach are provided in the last two subsections.

Implementation details. We run our experiments on a PC with an NVIDIA GeForce GTX 1080Ti GPU, a 4.2 GHz Intel Core i7-7700K CPU and 16 GB RAM. Our optimized code takes about 12 s per 3D human scan, which divides to 5-8 s for the multi-stage human template alignment (about 1.5, 2, and 3 s for each stage, respectively), 0.5 s for the tightness map prediction and 0.5 s for the shape recovery from tightness. All the energy functions of the multi-stage alignment are solved via a GPU-based Conjugate Gradient solver. In all experiments, we use the following empirically determined parameters: $N_{\mathbf{G}^S} = 1407$, $\lambda_{reg}^S = 10$; $N_{\mathbf{G}^D} = 2103$, $\lambda_{reg}^V = 7$ $\lambda_{point}^D = 0.5$, $\lambda_{plane}^D = 1.5$; $\lambda_{reg}^V = 1$, $\lambda_{point}^V = 1$ and $\lambda_{plane}^V = 1.5$. For the tightness prediction, we set the resolution of clothed-GI as 224×224. Note that the clothing
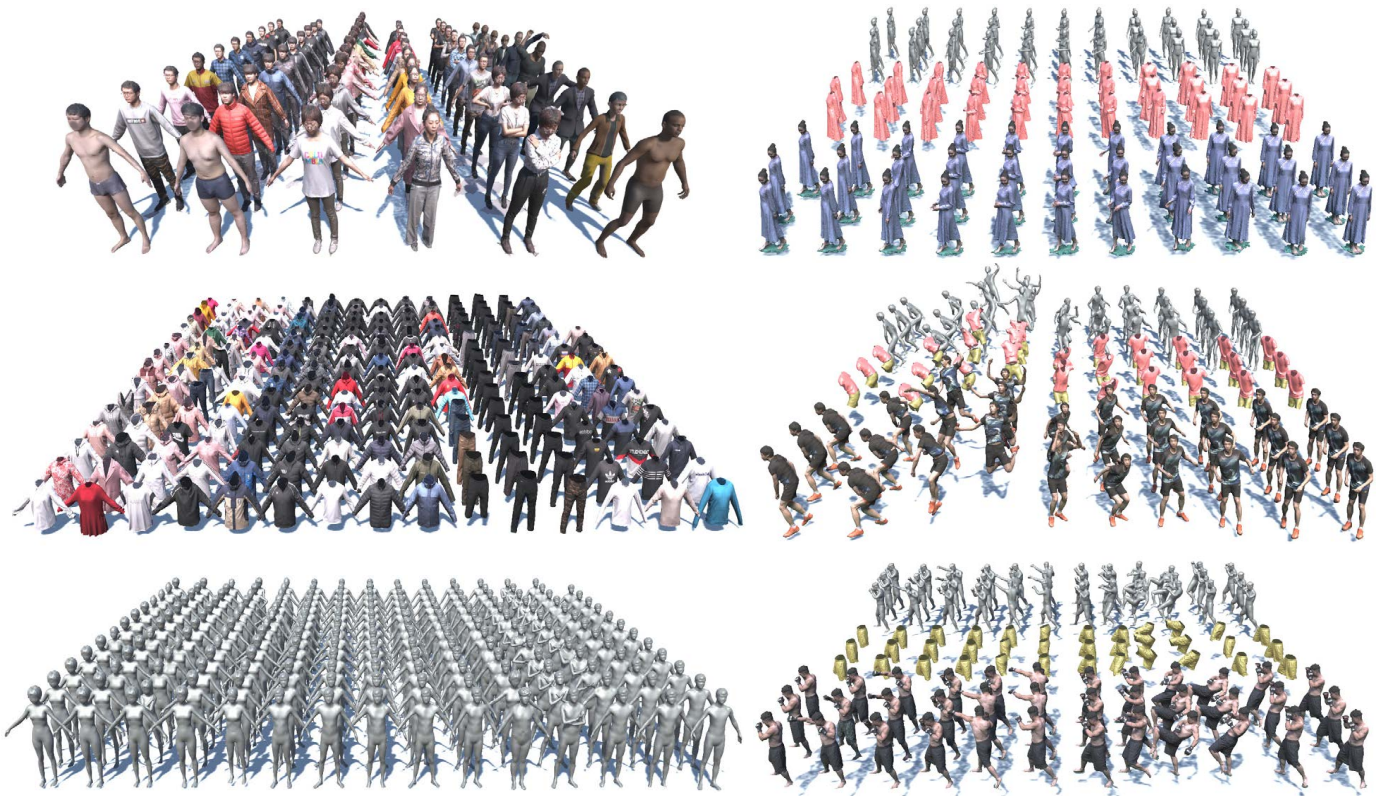
Fig. 8: The gallery of our Clothing Tightness Dataset (CTD). First column from top to bottom: 1) Sampling of various clothed human, including synthetic models (rightmost) and two body shape scans. 2) Various segmented clothes with 'A' pose only. 3) Carven body shapes with 'A' pose only. Second column are three typical dynamic sequences in our dataset including clothed human, segmented clothes, and carven body shapes.

Fig. 9: The gallery of our results. From down to top, the captured meshes, predicted tightness, recovered body shapes and segmented clothes.

tightness predictor is pre-trained on our dataset, which takes about 3 hours, and the training on CTD needs 4 hours.

6.1 Dataset

For a thorough evaluation of our method, we utilize both the most popular public dataset and a much larger captured dataset for the task of reconstructing both the human body shape and garments.
Bodies Under Flowing Fashion Dataset. The BUFF dataset [63] is the most popular public dataset for body shape estimation,

which contains three males and three females models wearing two types of clothing (t-shirt/long pants and a soccer outfit). It provides a dynamic sequence for each subject but only with the per-vertex color rather than extra high-quality RGB textures. BUFF also contains the body shapes under general T pose without garments as the ground truth. Since the data size of BUFF is far from enough to train our tightness prediction network, we only utilize the sampling frames from their scans as input and predict the tightness with the pre-trained model using our dataset.
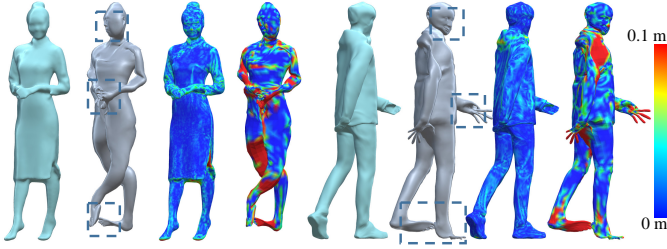
Fig. 10: The comparison between our enhanced clothing-adapted SMPL (CA-SMPL) and the original SMPL [30] for the clothing alignment. The green meshes are the results of our alignment algorithm using our enhanced SMPL, while the gray meshes are the results of the same algorithm using SMPL. The alignment error is color coded from blue to red.

Clothing Tightness Dataset (CTD). To model clothing tightness in a data-driven manner, we propose a new benchmark dataset, which contains 880 dressed human meshes with both the body geometry and segmented individual pieces of garments. Among them, 228 meshes are statically captured, and 652 are from dynamic 3D human sequences (13 sequences in total). We have captured 18 subjects, 9 males and 9 females, 10 of them are with the canonical "A" or "T" poses and 8 subjects are under free movements. For garment modeling, our CTD contains 228 different garments for each static caption, including T/long shirt, short/long/down coat, hooded jacket, pants, and skirt/dress, ranging from ultra-tight to puffy. For each dynamic sequence, we capture 400˜500 frames under 30 fps and evenly sample 40˜50 frames for our dataset. Note that most 3D meshes are reconstructed via a dome system equipped with 80 RGB cameras using the MVS approach [44], with about 50,000 vertices, 100,000 facets, and a 4K texture, while few 3D meshes are reconstructed via the DynamicFusion approach [34] with very similar quality. The corresponding ground truth naked human shapes are obtained via the same system, and then 5 artists further manually segment each piece of clothing and carve the body shape out from the raw mesh. We then generate the ground truth tightness using the novel formulation in Sec.5.1. Fig. 7 illustrates the high-quality examples from our dataset, while Fig. 8 further provides the gallery of our whole dataset. We will make our dataset publicly available. To train our tightness prediction network in Sec. 5.2, we utilize 80% of the dataset as training set, and the others as testing set. We also generate 800 hundred clothed human meshes with synthetic avatars using Adobe Fuse CC for the pre-training of our network. Fig. 9 demonstrated the multi-layer results of our approach, where both the human body shape and the garments under various clothing tightness and human postures are faithful reconstructions.

6.2 Evaluation

In this section, we evaluate our individual technique components, i.e., the human template alignment, the clothing tightness prediction, as well as the shape recovery from the tightness map in the following contents, respectively.

Alignment evaluation. We first evaluate the effectiveness of our clothing-adaptive human template (CA-SMPL) in Sec. 4.1 by comparing to the original SMPL model [30] using the same multi-stage alignment algorithm. As shown in Fig.10, the original SMPL suffers from severe alignment error, especially for those local
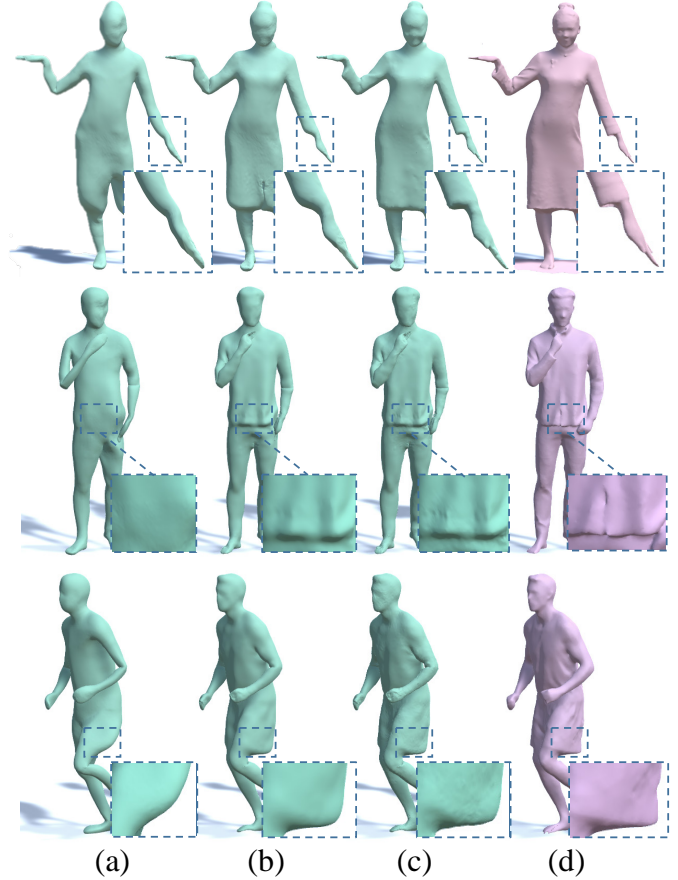

Fig. 11: The qualitative evaluation of our multi-stage alignment methods. (a) The results after silhouette based alignment. (b) The results after point cloud based alignment. (c) The results after per-vertex alignment. (d) The captured meshes (Target meshes).

Method	Mean↓	RMS↓	Error (mm)↓
Non-rigid [49]	0.448%	0.762%	13.44
Silhouette based [55]	0.494%	0.779%	14.82
Point cloud based	0.286%	0.585%	8.58
Ours	**0.263%**	**0.521%**	**7.89**

TABLE 1: Comparison of alignment methods for clothed human mesh. *Non-rigid* [49] is a baseline to directly align a 3D scanned mesh with the input point cloud. *Silhouette based* [55] is a baseline to align a 3D mesh from silhouette only, which is also our first stage. *Point cloud based* is our second stage using the results of the first stage as an initial value. ↓ means the smaller is better. *Mean* and *Root-Mean-Square (RMS)* are the metrics of Hausdorff distance [12], normalized with the bounding box diagonal of all clothed meshes, which is 3 in our setting. *Error (mm)* represents the per-vertex error with millimeter, using the same Hausdorff distance.

regions like faces and fingers due to the limited generation ability to handle clothing variations. In contrast, our enhanced template is more robust to both the clothing and human posture variations, leading to superior alignment accuracy.

We further evaluate our multi-stage alignment in Sec. 4.2 by analyzing the influence of each stage, both qualitatively and quantitatively. Let *Silhouette based* and *Point cloud based* denote the variations of our alignment method after the first and the
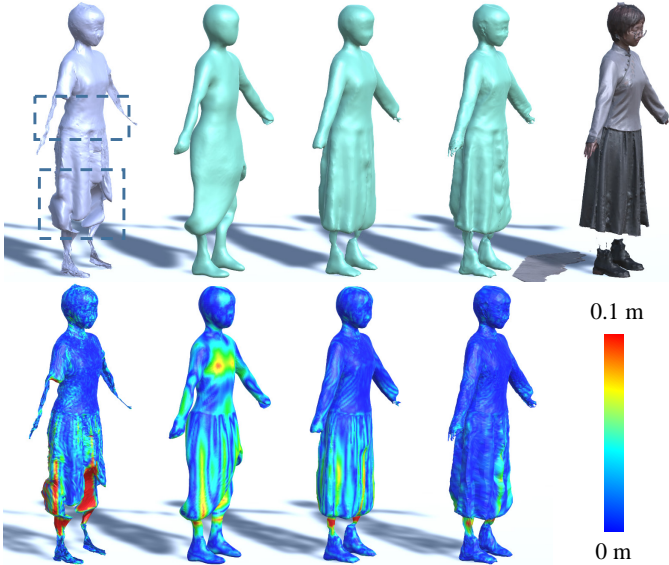
Fig. 12: The comparison between our method and non-rigid method on per-vertex error. Non-rigid method [49] is a baseline to directly align a 3D mesh with the captured mesh. From left to right, aligned mesh using only non-rigid method [49], our aligned mesh with silhouette, our aligned mesh with point cloud, our final aligned mesh, and target clothed mesh. The second column is per-vertex alignment error colored from blue (good) to red (bad).

Method	SSIM↑	L1/L2↓	mask IoU↑
Baseline L2	62.27%	0.281%	90.17%
OptCuts L1	43.91%	0.4929%	88.20%
Ours L1	**67.24%**	**0.2223%**	**93.89%**

TABLE 2: Evaluation of our TightNet. ↑ means the larger is better, while ↓ means the smaller is better.

second stages, respectively. Besides, we further compare to the alignment baseline [49], which directly align a 3D mesh with the input point cloud, denoted as *Non-rigid*. In Fig.11 we present the qualitative results of each stage for various challenging inputs. Note that our full scheme achieves superior alignment results and can even float the crack on skirt and match the clothing boundary around the wrist. Furthermore, the qualitative and quantitative results in Fig. 12 clearly demonstrate the effectiveness of each stage in our alignment scheme. Meanwhile, without the good initial state provided by the silhouette based deformation, the baseline [49] can not converge to a good result.

For further quantitative evaluation on our dataset, we utilize Metro [12], which is based on Hausdorff distance for comparing the difference of two meshes, and calculate its normalized *Mean* and *Root-Mean-Square (RMS)* as the metrics with a normalized factor (3 in our setting). We also calculate the per-vertex error as a relative quantitative metric, denoted as *Error (mm)*. Tab.1 shows that our full pipeline consistently outperforms the other baseline variations in terms of all these quantitative metrics. This not only highlights the contribution of each alignment stage but also illustrates that our approach can robustly align the enhanced human template to the input 3D scan.

TightNet evaluation. Here, we evaluate our TightNet quantitatively by comparing with two variation baselines using L2 loss or OptCut [28] for 2D mapping, denoted as *Baseline L2* and *OptCuts*
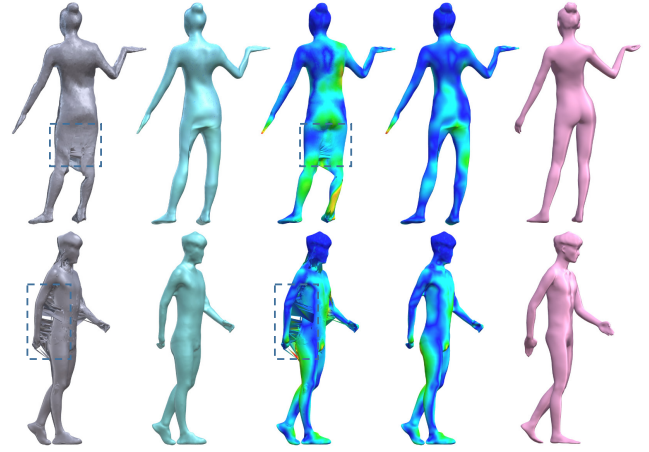

Fig. 13: Evaluation of our shape recovery scheme. From left to right: the recovered body before (gray) and after (green) our shape optimization in Eq.(18); the corresponding per-vertex errors which are color-coded from blue to red; the ground-truth bodies (red).
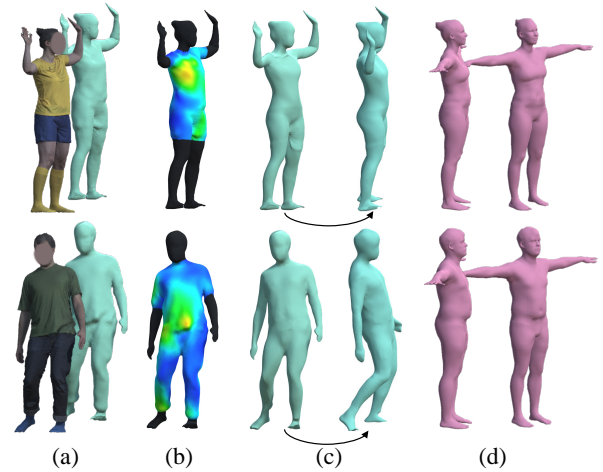

Fig. 14: Comparison with our recovered body shapes and Zhang *et al*. [63] in BUFF Dataset. (a) Input Meshes and aligned meshes. (b) Predicted tightness on meshes. (c) The recovered body shape of our results. (d) The results of Zhang *et al*. [63].

L1, respectively. We utilize the L1 norm and the structural similarity (SSIM) [51] for predicting the perceived quality of images, with window size (11 in our setting) to avoid the unreasonable effectiveness [64]. To evaluate the garment mask prediction, we utilize the mask IoU with a threshold 0.5 since the mask output of TightNet is 0 to 1 initially. As shown in Tab.2, our TightNet with L1 loss and geometry image for 2D mapping achieves the highest accuracy, leading to more robust multi-layer reconstruction from only a single 3D scan.

Shape recovery evaluation. We evaluate our optimization-based shape recovery scheme by comparing it with the baseline variation using the straight-forward solution in Eq.(17). As shown in Fig.13, the variation suffers from inferior reconstruction results, especially in the local regions around the oxter and crotch. In contrast, our shape recovery scheme successfully compresses the tightness error so as to provide accurate and visually pleasant body shape reconstruction results.
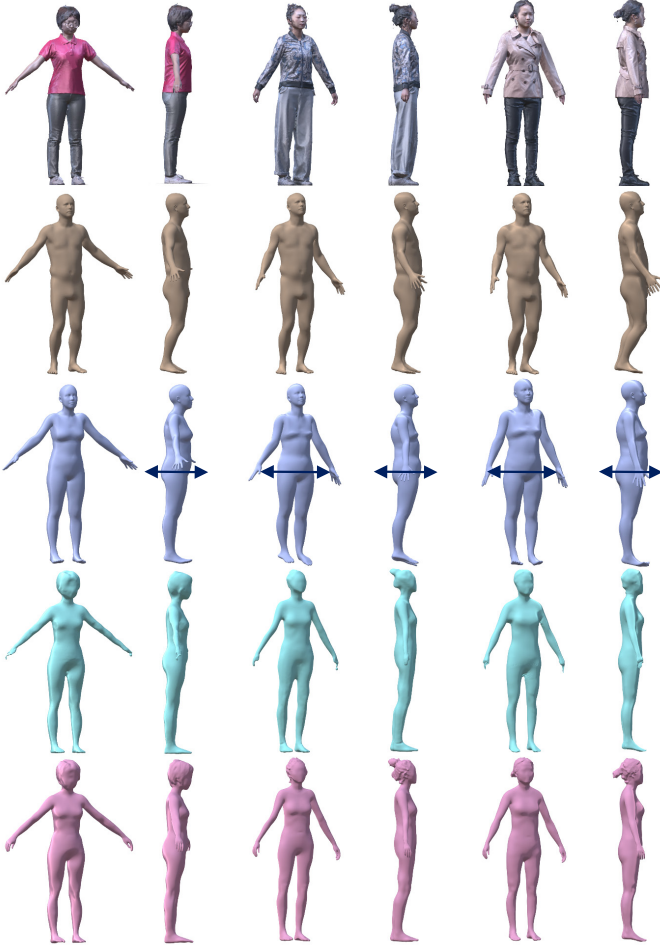
Fig. 15: The comparison of recovered body shapes in our Clothing Tightness Dataset (CTD). From top to down: The input mesh; the recovered bodies using image based method HMR [23], mesh-based method DoubleFusion [61] and our method; the ground truth bodies. The black arrows indicate the results of DoubleFusion are always fatter with the influence of clothing.

Input	Method	Mean↓	RMS↓	Error (mm)↓	Front IoU↑	Side IoU↑
Image	HMR [23]	1.607%	2.195%	48.21	74.70%	67.51%
	SMPL-X [39]	1.478%	2.121%	44.34	78.76%	60.54%
Mesh	DoubleFusion [61]	0.804%	0.996%	24.12	82.49%	77.29%
	Our	**0.191%**	**0.451%**	**5.73**	**90.12%**	**94.29%**

TABLE 3: Comparison of recovered body shapes in CTD. *Mean, Root-Mean-Square (RMS)*, and *Error (mm)* are same as Tab.1. *Front IoU* represents the mean IoU of each projected mask pairs (estimated body and ground-truth body) from the view of input image for HMR [23] and SMPL-X [39]. *Side IoU* uses same metric like *Front IoU* but projected from the sideview.
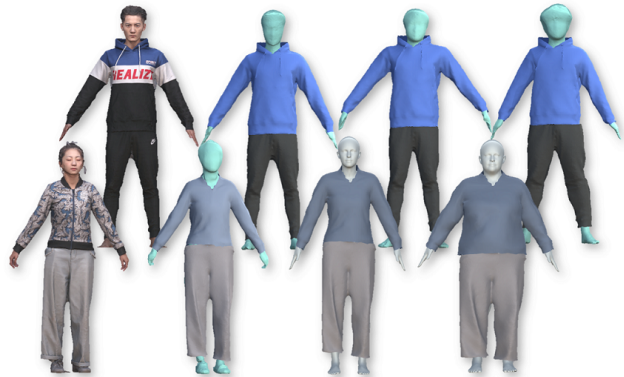

Fig. 16: The application of cloth retargeting. From left to right: the input MVS meshes; the estimated body shape and segmented garments; the retargeted clothing with slim body and fat body, respectively. Note that our enhanced template models are in green while the original SMPL [30] models are in gray.

6.3 Comparisons of Body Recovery

In this subsection, we demonstrate the overall performance of the proposed approach by comparing it against other state-of-the-art mesh-based and image-based body recovery methods, both qualitatively and quantitatively. For mesh-based comparison, we compare to the state-of-the-art approaches, including the one proposed by Zhang *et al*. [63] and the volumetric optimization stage of DoubleFusion [61]. The former one utilizes a sequence of dressed mesh as input to recover body shape while the latter DoubleFusion [61] optimizes the body shape from a single volumetric mesh input. For the image-based comparison, we compare to HMR [23] and SMPL-X [39], which regress the human model directly from only a single RGB image input.

As shown in Fig. 14, we achieve a competitive result against the sequence-based method of Zhang *et al*. [63] on the BUFF dataset. Note that our method only uses a single 3D scan as input rather than a dynamic sequence of human models, which is hard to obtain for the daily applications. Besides, our network is only pre-trained using our dataset CTD without fine-tuning on BUFF, which demonstrates the generation ability for our approach to recover both human body shape and garments from only a single 3D scan.

Then, we utilize our dataset CTD with ground-truth annotations for further qualitative and quantitative comparisons. In Fig. 15, we provide a qualitative comparison to DoubleFusion [61] and HMR [23] on three challenging cases with various clothing tightness and similar postures to get rid of the posture ambiguity. DoubleFusion [61] suffers from inferior shape recovery and turns to estimate fatter human body without considering the clothing tightness, while HMR [23] suffers from scale ambiguity to provide only visually pleasant rather than accurate human body shape, which is the inherent issue of such image-based methods. In contrast, our approach accurately reconstructs the human body shape by modeling various clothing tightness effectively.

The quantitative comparison on the dataset CTD against both the mesh-based and image-based methods is provided in Tab.3, in terms of the *Mean* and *Root-Mean-Square (RMS)* from Metro [12] as well as the per-vertex error *Error (mm)*. Besides, we calculate the mean IoU of each projected mask pairs (estimated body and ground-truth body) from the view of rendered image for image-based methods, denoted as *Front IoU*. We also utilize *Side IoU* with the same operation like *Front IoU* projected from a side-view for thorough analysis. As shown in Tab.3, our approach achieves significantly much more accurate body recovery results in terms of all the metrics above, with the aid of modeling the influence of clothing tightness. Besides, all these comparisons against different input modularities not only highlight the robustness of our approach but also demonstrates the uniqueness of our approach as a good compromising settlement between over-demanding input data resources and highly accurate reconstruction.

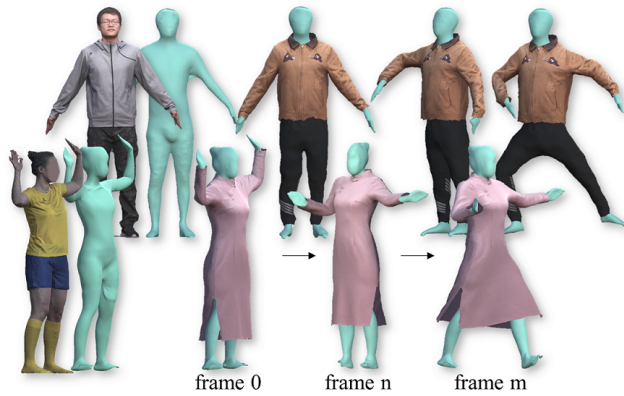frame 0   frame n   frame m

Fig. 17: The application of clothed avatar animation. From left to right: The input meshes and our recovered inner body shape; our cloth retargeting results; our multi-layer avatar animation results into various human postures.

6.4 Application

In this subsection, based on our high quality multi-layer reconstruction, we further demonstrate various interesting applications of our approach, including immersive cloth retargeting and clothed avatar animation.

Cloth retargeting. Recall that in our approach, thanks to our novel clothing tightness formulation, both the aligned human template to the dressed scan in Sec. 4.2 and the recovered body shape in Sec. 5.3 share the same mesh topology and the rigged skeleton as our enhanced human template in Sec. 4.1. Note that such displacements between the aligned template and its recovered body shape are our predicted clothing tightness. Thus, we can directly transfer the clothing to various recovered body shapes in terms of cloth-to-body and body-to-body displacements. As shown in Fig.16, we can achieve highly immersive cloth retargeting, and even fit our enhanced human template back to the original SMPL [30] so as to transfer the clothing to shape-variant SMPL model directly.

Clothed avatar animation. Benefiting from our enhanced human template with rigged skeleton and the novel clothing tightness formulation, we are able to reconstruct a consistent multi-layer avatar from the input 3D scan to infer the body shape and the various segmented garments. Thus, we can not only change the garments of current human target by using various clothing tightness, but also further animate the dressed avatar naturally by driving its inner body with various postures and maintaining current clothing tightness. As shown in Fig. 17, we can achieve realistic clothed avatar animation, without extra physical simulation for the clothing.

6.5 Limitations and Discussion

Though our approach is effective for body shape and garment reconstruction from only a single 3D scan, it sill owns limitations as follows. First, we cannot handle extreme human poses such as crossing legs/arms or curling up, or very low-quality scans, which we plan to address by incorporating extra data-driven human keypoint priors to provide a good initialization. Our current clothing tightness formulation still cannot simulate the dynamic movement of clothing in a physically plausible manner for our reconstructed garments. It's a promising direction to further model the clothing tightness for 4D dynamic sequences with the aid of extra human

motion priors. Besides, currently utilized geometry images in our approach can only handle genus 0 human geometry. In reality, the human model can have very complex topology, and a much more sophisticated geometry image generation approach is required. Alignment schemes that can handle topologically complex human models are our immediate future work. Our approach relies on raw 3D human scans, which are usually difficult to obtain, and the quality can not be guaranteed. Hence we plan to explore the possibility of directly taking a single or sparse set of 2D images as the input of the MVS setting for recovering the 3D clothing and human shape. Also, through augmented training under various lighting conditions using the light stage, it is possible to capture the reflection property of the clothing and for better AR/VR or try-on experience.

7 CONCLUSION

We present TightCap, a learning-based scheme for robustly and accurately capturing the clothing tightness as well as human geometry with a single clothed 3D human raw mesh. The key contribution of our approach is the usage of geometry image for tightness prediction, and the alignment of human geometry enables the geometry image correspondence from various types of clothing. Moreover, we collect a large 3D Clothing Tightness Dataset (CTD) for the clothed human reconstruction tasks. We propose and train a modified conditional GAN network to automatically predict the clothing tightness and, subsequently, the underlying human shape. Experiments demonstrate the reliability and accuracy of our method. We also exhibit two interesting virtual try-on applications, i.e., cloth retargeting and clothed avatar animation. We believe our scheme will benefit various AR/VR research and applications, such as virtual try-on and avatar animation.

REFERENCES

[1] T. Alldieck, M. Magnor, B. L. Bhatnagar, C. Theobalt, and G. Pons-Moll. Learning to reconstruct people in clothing from a single RGB camera. In *IEEE Conference on Computer Vision and Pattern Recognition (CVPR)*, jun 2019.

[2] T. Alldieck, M. Magnor, W. Xu, C. Theobalt, and G. Pons-Moll. Video based reconstruction of 3d people models. In *Proceedings of the IEEE Conference on Computer Vision and Pattern Recognition*, pages 8387–8397, 2018.

[3] R. Alp Güler, N. Neverova, and I. Kokkinos. Densepose: Dense human pose estimation in the wild. In *Proceedings of the IEEE Conference on Computer Vision and Pattern Recognition*, pages 7297–7306, 2018.

[4] D. Anguelov, P. Srinivasan, D. Koller, S. Thrun, J. Rodgers, and J. Davis. Scape: Shape completion and animation of people. *ACM Transactions on Graphics (TOG)*, 24(3):408–416, 2005.

[5] S. Baker, T. Kanade, et al. Shape-from-silhouette across time part ii: Applications to human modeling and markerless motion tracking. *International Journal of Computer Vision*, 63(3):225–245, 2005.

[6] A. O. Bălan and M. J. Black. The naked truth: Estimating body shape under clothing. In *Proceedings of the European Conference on Computer Vision*, pages 15–29. Springer, 2008.

[7] B. L. Bhatnagar, G. Tiwari, C. Theobalt, and G. Pons-Moll. Multi-garment net: Learning to dress 3d people from images. In *Proceedings of the IEEE International Conference on Computer Vision*, pages 5420–5430, 2019.

[8] F. Bogo, M. J. Black, M. Loper, and J. Romero. Detailed full-body reconstructions of moving people from monocular rgb-d sequences. In *Proceedings of the IEEE International Conference on Computer Vision*, pages 2300–2308, 2015.

[9] Z. Cao, T. Simon, S.-E. Wei, and Y. Sheikh. Realtime multi-person 2d pose estimation using part affinity fields. In *Proceedings of the IEEE Conference on Computer Vision and Pattern Recognition*, 2017.

[10] G. K. Cheung, S. Baker, and T. Kanade. Visual hull alignment and refinement across time: A 3d reconstruction algorithm combining shape-from-silhouette with stereo. In *2003 IEEE Computer Society Conference on Computer Vision and Pattern Recognition, 2003. Proceedings.*, volume 2, pages II–375. IEEE, 2003.

[11] K. Cheung, S. Baker, and T. Kanade. Shape-from-silhouette of articulated objects and its use for human body kinematics estimation and motion capture. In *2003 IEEE Computer Society Conference on Computer Vision and Pattern Recognition, 2003. Proceedings.*, volume 1, pages I–I. IEEE, 2003.

[12] P. Cignoni, C. Rocchini, and R. Scopigno. Metro: measuring error on simplified surfaces. In *Computer graphics forum*, volume 17, pages 167–174. Wiley Online Library, 1998.

[13] A. Collet, M. Chuang, P. Sweeney, D. Gillett, D. Evseev, D. Calabrese, H. Hoppe, A. Kirk, and S. Sullivan. High-quality streamable free-viewpoint video. *ACM Transactions on Graphics (ToG)*, 34(4):69, 2015.

[14] S. Corazza, L. Muendermann, A. Chaudhari, T. Demattio, C. Cobelli, and T. P. Andriacchi. A markerless motion capture system to study musculoskeletal biomechanics: visual hull and simulated annealing approach. *Annals of biomedical engineering*, 34(6):1019–1029, 2006.

[15] M. Dou, S. Khamis, Y. Degtyarev, P. Davidson, S. R. Fanello, A. Kowdle, S. O. Escolano, C. Rhemann, D. Kim, J. Taylor, et al. Fusion4d: Real-time performance capture of challenging scenes. *ACM Transactions on Graphics (TOG)*, 35(4):114, 2016.

[16] Y. Furukawa, C. Hernández, et al. Multi-view stereo: A tutorial. *Foundations and Trends® in Computer Graphics and Vision*, 9(1-2):1–148, 2013.

[17] X. Gu, S. J. Gortler, and H. Hoppe. Geometry images. *ACM Transactions on Graphics (TOG)*, 21(3):355–361, 2002.

[18] N. Hasler, C. Stoll, B. Rosenhahn, T. Thormählen, and H.-P. Seidel. Estimating body shape of dressed humans. *Computers & Graphics*, 33(3):211–216, 2009.

[19] P. Isola, J.-Y. Zhu, T. Zhou, and A. A. Efros. Image-to-image translation with conditional adversarial networks. In *Proceedings of the IEEE Conference on Computer Vision and Pattern Recognition*, pages 1125–1134, 2017.

[20] B. Jiang, J. Zhang, Y. Hong, J. Luo, L. Liu, and H. Bao. Bcnet: Learning body and cloth shape from a single image. *arXiv preprint arXiv:2004.00214*, 2020.

[21] H. Joo, T. Simon, X. Li, H. Liu, L. Tan, L. Gui, S. Banerjee, T. Godisart, B. Nabbe, I. Matthews, et al. Panoptic studio: A massively multiview system for social interaction capture. *IEEE Transactions on Pattern Analysis and Machine Intelligence*, 41(1):190–204, 2019.

[22] H. Joo, T. Simon, and Y. Sheikh. Total capture: A 3d deformation model for tracking faces, hands, and bodies. In *Proceedings of the IEEE Conference on Computer Vision and Pattern Recognition*, pages 8320–8329, 2018.

[23] A. Kanazawa, M. J. Black, D. W. Jacobs, and J. Malik. End-to-end recovery of human shape and pose. In *Proceedings of the IEEE Conference on Computer Vision and Pattern Recognition*, pages 7122–7131, 2018.

[24] Z. Lahner, D. Cremers, and T. Tung. Deepwrinkles: Accurate and realistic clothing modeling. In *Proceedings of the European Conference on Computer Vision*, pages 667–684, 2018.

[25] Z. Lahner, D. Cremers, and T. Tung. Deepwrinkles: Accurate and realistic clothing modeling. In *Proceedings of the European Conference on Computer Vision (ECCV)*, pages 667–684, 2018.

[26] C. Lassner, G. Pons-Moll, and P. V. Gehler. A generative model of people in clothing. In *Proceedings of the IEEE International Conference on Computer Vision*, pages 853–862, 2017.

[27] C. Lassner, J. Romero, M. Kiefel, F. Bogo, M. J. Black, and P. V. Gehler. Unite the people: Closing the loop between 3d and 2d human representations. In *Proceedings of the IEEE Conference on Computer Vision and Pattern Recognition*, pages 6050–6059, 2017.

[28] M. Li, D. M. Kaufman, V. G. Kim, J. Solomon, and A. Sheffer. Optcuts: Joint optimization of surface cuts and parameterization. *ACM Transactions on Graphics (TOG)*, 37(6), 2018.

[29] O. Litany, A. Bronstein, M. Bronstein, and A. Makadia. Deformable shape completion with graph convolutional autoencoders. In *The IEEE Conference on Computer Vision and Pattern Recognition (CVPR)*, June 2018.

[30] M. Loper, N. Mahmood, J. Romero, G. Pons-Moll, and M. J. Black. Smpl: A skinned multi-person linear model. *ACM Transactions on Graphics (TOG)*, 34(6):248, 2015.

[31] Q. Ma, J. Yang, A. Ranjan, S. Pujades, G. Pons-Moll, S. Tang, and M. Black. Learning to dress 3d people in generative clothing. In *IEEE Conference on Computer Vision and Pattern Recognition (CVPR)*. IEEE, jun 2020.

[32] M. Mikhnevich and P. Hebert. Shape from silhouette under varying lighting and multi-viewpoints. In *2011 Canadian Conference on Computer and Robot Vision*, pages 285–292. IEEE, 2011.

[33] A. Neophytou and A. Hilton. A layered model of human body and garment deformation. In *2014 2nd International Conference on 3D Vision*, volume 1, pages 171–178. IEEE, 2014.

[34] R. A. Newcombe, D. Fox, and S. M. Seitz. Dynamicfusion: Reconstruction and tracking of non-rigid scenes in real-time. In *Proceedings of the IEEE Conference on Computer Vision and Pattern Recognition*, pages 343–352, 2015.

[35] R. A. Newcombe, S. Izadi, O. Hilliges, D. Molyneaux, D. Kim, A. J. Davison, P. Kohi, J. Shotton, S. Hodges, and A. Fitzgibbon. Kinectfusion: Real-time dense surface mapping and tracking. In *Proceedings of the IEEE International Symposium on Mixed and Augmented Reality*, pages 127–136. IEEE, 2011.

[36] R. A. Newcombe, S. J. Lovegrove, and A. J. Davison. Dtam: Dense tracking and mapping in real-time. In *Proceedings of the IEEE International Conference on Computer Vision*, pages 2320–2327. IEEE, 2011.

[37] A. Newell, K. Yang, and J. Deng. Stacked hourglass networks for human pose estimation. In *Proceedings of the European Conference on Computer Vision*, pages 483–499. Springer, 2016.

[38] C. Patel, Z. Liao, and G. Pons-Moll. Tailornet: Predicting clothing in 3d as a function of human pose, shape and garment style. In *IEEE Conference on Computer Vision and Pattern Recognition (CVPR)*. IEEE, jun 2020.

[39] G. Pavlakos, V. Choutas, N. Ghorbani, T. Bolkart, A. A. A. Osman, D. Tzionas, and M. J. Black. Expressive body capture: 3d hands, face, and body from a single image. In *Proceedings IEEE Conf. on Computer Vision and Pattern Recognition (CVPR)*, 2019.

[40] G. Pavlakos, L. Zhu, X. Zhou, and K. Daniilidis. Learning to estimate 3d human pose and shape from a single color image. In *Proceedings of the IEEE Conference on Computer Vision and Pattern Recognition*, pages 459–468, 2018.

[41] L. Pishchulin, E. Insafutdinov, S. Tang, B. Andres, M. Andriluka, P. V. Gehler, and B. Schiele. Deepcut: Joint subset partition and labeling for multi person pose estimation. In *Proceedings of the IEEE Conference on Computer Vision and Pattern Recognition*, pages 4929–4937, 2016.

[42] G. Pons-Moll, S. Pujades, S. Hu, and M. J. Black. Clothcap: Seamless 4d clothing capture and retargeting. *ACM Transactions on Graphics (TOG)*, 36(4):73, 2017.

[43] O. Ronneberger, P. Fischer, and T. Brox. U-net: Convolutional networks for biomedical image segmentation. In *International Conference on Medical image computing and computer-assisted intervention*, pages 234–241. Springer, 2015.

[44] J. L. Schönberger, E. Zheng, J.-M. Frahm, and M. Pollefeys. Pixelwise view selection for unstructured multi-view stereo. In *Proceedings of the European Conference on Computer Vision*, pages 501–518. Springer, 2016.

[45] T. Simon, H. Joo, I. Matthews, and Y. Sheikh. Hand keypoint detection in single images using multiview bootstrapping. In *Proceedings of the IEEE Conference on Computer Vision and Pattern Recognition*, 2017.

[46] O. Sorkine and M. Alexa. As-rigid-as-possible surface modeling. In *Proceedings of the Symposium on Geometry Processing*, volume 4, pages 109–116, 2007.

[47] C. Strecha, W. Von Hansen, L. Van Gool, P. Fua, and U. Thoennessen. On benchmarking camera calibration and multi-view stereo for high resolution imagery. In *Proceedings of the IEEE Conference on Computer Vision and Pattern Recognition*, pages 1–8. Ieee, 2008.

[48] R. W. Sumner, J. Schmid, and M. Pauly. Embedded deformation for shape manipulation. *ACM Transactions on Graphics (TOG)*, 26(3):80, 2007.

[49] J. Tong, J. Zhou, L. Liu, Z. Pan, and H. Yan. Scanning 3d full human bodies using kinects. *IEEE transactions on visualization and computer graphics*, 18(4):643–650, 2012.

[50] B. Triggs, P. F. McLauchlan, R. I. Hartley, and A. W. Fitzgibbon. Bundle adjustment — a modern synthesis. In *Proceedings of the International Workshop on Vision Algorithms*, pages 298–372. Springer, 1999.

[51] Z. Wang, A. C. Bovik, H. R. Sheikh, and E. P. Simoncelli. Image quality assessment: from error visibility to structural similarity. *IEEE transactions on image processing*, 13(4):600–612, 2004.

[52] S.-E. Wei, V. Ramakrishna, T. Kanade, and Y. Sheikh. Convolutional

pose machines. In *Proceedings of the IEEE Conference on Computer Vision and Pattern Recognition*, pages 4724–4732, 2016.

[53] S. Wuhrer, L. Pishchulin, A. Brunton, C. Shu, and J. Lang. Estimation of human body shape and posture under clothing. *Computer Vision and Image Understanding*, 127:31–42, 2014.

[54] D. Xiang, H. Joo, and Y. Sheikh. Monocular total capture: Posing face, body, and hands in the wild. In *Proceedings of the IEEE Conference on Computer Vision and Pattern Recognition*, 2019.

[55] W. Xu, A. Chatterjee, M. Zollhoefer, H. Rhodin, D. Mehta, H.-P. Seidel, and C. Theobalt. Monoperfcap: Human performance capture from monocular video. *ACM Transactions on Graphics (TOG)*, 37(2):27, 2018.

[56] Y. Xu, S.-C. Zhu, and T. Tung. Denserac: Joint 3d pose and shape estimation by dense render-and-compare. In *Proceedings of the IEEE International Conference on Computer Vision*, pages 7760–7770, 2019.

[57] J. Yang, J.-S. Franco, F. Hétroy-Wheeler, and S. Wuhrer. Estimation of human body shape in motion with wide clothing. In *Proceedings of the European Conference on Computer Vision*, pages 439–454. Springer, 2016.

[58] J. Yang, J.-S. Franco, F. Hétroy-Wheeler, and S. Wuhrer. Analyzing clothing layer deformation statistics of 3d human motions. In *Proceedings of the European Conference on Computer Vision*, pages 237–253, 2018.

[59] T. Yu, K. Guo, F. Xu, Y. Dong, Z. Su, J. Zhao, J. Li, Q. Dai, and Y. Liu. Bodyfusion: Real-time capture of human motion and surface geometry using a single depth camera. In *Proceedings of the IEEE International Conference on Computer Vision*, pages 910–919, 2017.

[60] T. Yu, Z. Zheng, K. Guo, J. Zhao, Q. Dai, H. Li, G. Pons-Moll, and Y. Liu. Doublefusion: Real-time capture of human performances with inner body shapes from a single depth sensor. In *Proceedings of the IEEE Conference on Computer Vision and Pattern Recognition*, pages 7287–7296, 2018.

[61] T. Yu, Z. Zheng, K. Guo, J. Zhao, Q. Dai, H. Li, G. Pons-Moll, and Y. Liu. Doublefusion: Real-time capture of human performances with inner body shapes from a single depth sensor. In *Proceedings of the IEEE conference on computer vision and pattern recognition*, pages 7287–7296, 2018.

[62] T. Yu, Z. Zheng, Y. Zhong, J. Zhao, Q. Dai, G. Pons-Moll, and Y. Liu. Simulcap: Single-view human performance capture with cloth simulation. In *2019 IEEE/CVF Conference on Computer Vision and Pattern Recognition (CVPR)*, pages 5499–5509. IEEE, 2019.

[63] C. Zhang, S. Pujades, M. J. Black, and G. Pons-Moll. Detailed, accurate, human shape estimation from clothed 3d scan sequences. In *Proceedings of the IEEE Conference on Computer Vision and Pattern Recognition*, pages 4191–4200, 2017.

[64] R. Zhang, P. Isola, A. A. Efros, E. Shechtman, and O. Wang. The unreasonable effectiveness of deep features as a perceptual metric. In *Proceedings of the IEEE Conference on Computer Vision and Pattern Recognition*, pages 586–595, 2018.

[65] Z. Zheng, T. Yu, Y. Wei, Q. Dai, and Y. Liu. Deephuman: 3d human reconstruction from a single image. In *Proceedings of the IEEE International Conference on Computer Vision*, pages 7739–7749, 2019.

Pang Anqi is a Postgraduate Student at the School of Information Science and Technology (SIST), ShanghaiTech University. His research interests include human pose estimation, multi-view human joint estimation and deep learning.

Wei Yang is an engineer at the Advanced Technology and Projects division, Google LLC. He received the BEng and MS degrees from the Huazhong University of Science and Technology and Harbin Institute of Technology respectively, and the PhD degree from the University of Delaware (UDel) in Dec. 2017. He previously worked as a scientist the DGene. Co and joined ATAP at Google in Jan. 2020. His research interests include computer vision and computer graphics, with special focus in computational photography and 3D reconstruction.

Lan Xu received the BS degree from the Department of Information and Communication, College of Information Science & Electronic Engineering, Zhejiang University, Hangzhou, China, in 2015. He is currently working toward the PhD degree in the Department of Electronic and Computer Engineering, Hong Kong University of Science and Technology, Hong Kong SAR.

Xin Chen is a Ph.D. student at the School of Information Science and Technology (SIST), ShanghaiTech University. He obtained his BEng degree from the School of Science at Qingdao University of Technology. His research interests include computer vision for graphics, with special focus in geometric deep learning, human performance caption, clothing models and dynamics, and image-based modeling. His homepage is https://chenxin.tech.

Jingyi Yu is the executive dean in the School of Information Science and Technology at ShanghaiTech University. He received B.S. from Caltech in 2000 and Ph.D. from MIT in 2005. He is also affiliated with the University of Delaware. His research interests span a range of topics in computer vision and computer graphics, especially on computational photography and non-conventional optics and camera designs. He is a recipient of the NSF CAREER Award, the AFOSR YIP Award, and the Outstanding Junior Faculty Award at the University of Delaware. He has served as general chair, program chair, and area chair of many international conferences such as CVPR, ICCV, ECCV, ICCP and NIPS. He is currently an Associate Editor of IEEE TPAMI, IEEE TIP and Elsevier CVIU, and will be program chair of ICPR 2020 and IEEE CVPR 2021.